THE UNIVERSITY of EDINBURGH

Edinburgh Research Explorer

Anion order in perovskite oxynitrides

Citation for published version:
Yang, M, Oro-Sole, J, Rodgers, JA, Belen Jorge, A, Fuertes, A & Attfield, JP 2011, 'Anion order in perovskite oxynitrides', *Nature Chemistry*, vol. 3, no. 1, pp. 47-52. https://doi.org/10.1038/NCHEM.908

Digital Object Identifier (DOI):
10.1038/NCHEM.908

Link:
Link to publication record in Edinburgh Research Explorer

Document Version:
Peer reviewed version

Published In:
Nature Chemistry

Publisher Rights Statement:
Copyright © 2011 Macmillan Publishers Limited. All rights reserved.

General rights
Copyright for the publications made accessible via the Edinburgh Research Explorer is retained by the author(s) and / or other copyright owners and it is a condition of accessing these publications that users recognise and abide by the legal requirements associated with these rights.

Take down policy
The University of Edinburgh has made every reasonable effort to ensure that Edinburgh Research Explorer content complies with UK legislation. If you believe that the public display of this file breaches copyright please contact openaccess@ed.ac.uk providing details, and we will remove access to the work immediately and investigate your claim.

OPEN ACCESS

Download date: 12. Oct. 2024

Post-print of peer-reviewed article published by the Nature Publishing Group.
Published article available at: http://dx.doi.org/10.1038/nchem.908

Cite as:
Yang, M., Oro-Sole, J., Rodgers, J. A., Belen Jorge, A., Fuertes, A., & Attfield, J. P. (2011). Anion order in perovskite oxynitrides. *Nature Chemistry*, 3(1), 47-52.

Manuscript received: 23/04/2010; Accepted: 14/10/2010; Article published: 28/11/2010

Anion order in perovskite oxynitrides**

Minghui Yang,[1] Judith Oró-Solé,[2] Jennifer A. Rodgers,[1] Ana Belén Jorge,[2] Amparo Fuertes[2] and J. Paul Attfield[1]

[1]Centre for Science at Extreme Conditions and School of Chemistry, University of Edinburgh, King's Buildings, Mayfield Road, Edinburgh, EH9 3JZ, UK.

[2]Institut de Ciència de Materials de Barcelona CSIC, Campus UAB, 08193 Bellaterra, Spain.

[*]Corresponding authors; J.P.A. e-mail: j.p.attfield@ed.ac.uk; A.F. e-mail: amparo.fuertes@icmab.es

[**]We thank M. Senn and C. Ritter for assistance with the neutron experiment at ILL. This work was supported by the Ministerio de Ciencia e Innovación (grants MAT2008-04587 and PR2008-0164), the Generalitat de Catalunya, the Engineering and Physical Science Research Council, the Science and Technology Facilities Council, the Royal Society, the Chemistry Research School of Edinburgh and St Andrews Universities and the Leverhulme Trust. We acknowledge the use of the Chemical Database Service at Daresbury.

Contributions:
J.P.A. and A.F. conceived and designed the study. Samples were prepared by A.B.J., J.O. and M.Y. J.O. recorded the electron diffraction images and J.O. and M.Y. performed the neutron diffraction experiment. Neutron diffraction data were analysed by M.Y. with guidance from J.P.A. and J.A.R. J.P.A. and A.F. co-wrote the manuscript with comments and contributions from the other authors.

Supporting information:
The authors declare no competing financial interests. Supplementary information accompanies this paper at www.nature.com/naturechemistry

Abstract

Transition-metal oxynitrides with perovskite-type structures are an emerging class of materials with optical, photocatalytic, dielectric and magnetoresistive properties that may be sensitive to oxide–nitride order, but the anion-ordering principles were unclear. Here we report an investigation of the representative compounds $SrMO_2N$ (M = Nb, Ta) using neutron and electron diffraction. This revealed a robust $1O/2(O_{0.5}N_{0.5})$ partial anion order (up to at least 750 °C in the apparently cubic high-temperature phases) that directs the rotations of MO_4N_2 octahedra in the room-temperature superstructure. The anion distribution is consistent with local *cis*-ordering of the two nitrides in each octahedron driven by covalency, which results in disordered zigzag M–N chains in planes within the perovskite lattice. Local structures for the full range of oxynitride perovskites are predicted and a future challenge is to tune properties by controlling the order and dimensionality of the anion chains and networks.

Main text

Transition-metal oxynitrides are an important class of emerging materials that, in optimal cases, may combine the advantages of oxides and nitrides. Generally, their stabilities in air and moisture are greater than those of the pure nitrides, but with smaller bandgaps than those of comparable oxides. This leads to useful electronic and/or optical properties, such as the N-doping of TiO_2 to tune the bandgap from the ultraviolet to the visible region for photocatalysis[1]. Many useful oxynitrides of high-valence (d^0 electron configuration) transition metals adopt the AMX_3 (X = N/O) perovskite-type crystal structure[2]; $CaTaO_2N$ and $LaTaON_2$ solid solutions are non-toxic, red–yellow pigments[3], $BaTaO_2N$ has a high dielectric constant[4] and photocatalyses the decomposition of water[5], and $EuNbO_2N$ and $EuWON_2$ are ferromagnetic and show colossal magnetoresistances (CMR)[6, 7].

The properties of perovskites are sensitive to small, structural distortions that may arise from tilting or electronic deformations of the MX_6 octahedra. Oxide/nitride anion order is also expected to be important, for example in directing the M-cation displacements in dielectric materials, but consistent models are not reported, even for representative oxynitride perovskites such as $SrMO_2N$ (M = Nb, Ta), in which the anion content is close to the ideal stoichiometry[2, 8, 9, 10]. Here, we report an investigation of anion order in these phases using variable-temperature neutron diffraction and electron diffraction. This revealed a robust, partial long-range anion order that is consistent with local *cis*-ordering of the two nitrides in each MO_4N_2 octahedron. The order directs the tilting of the octahedra in the low-temperature pseudotetragonal superstructure. The local anion order may be described as the formation of disordered zigzag M–N chains in two dimensions at low temperatures, changing towards three dimensions at high temperatures. These principles are applied to predict local structures across the range of $AMO_{3-x}N_x$ oxynitride perovskites.

Results

(i) Diffraction study

The cubic AMX_3 perovskite structure consists of a network of corner-linked MX_6 octahedra and ideally has cubic $Pm\bar{3}m$ symmetry, but this may be lowered through internal perturbations (including anion order) or rotations and tilts of the octahedra. This often leads to structural phase transitions such as those observed for $SrMO_2N$ (M = Nb, Ta). Additional superstructure diffraction peaks that arise from ordered rotations of the octahedra were seen at room temperature (Fig. 1), but only the peaks expected from a cubic perovskite were observed above 300 °C for $SrNbO_2N$ and above 200 °C for $SrTaO_2N$.

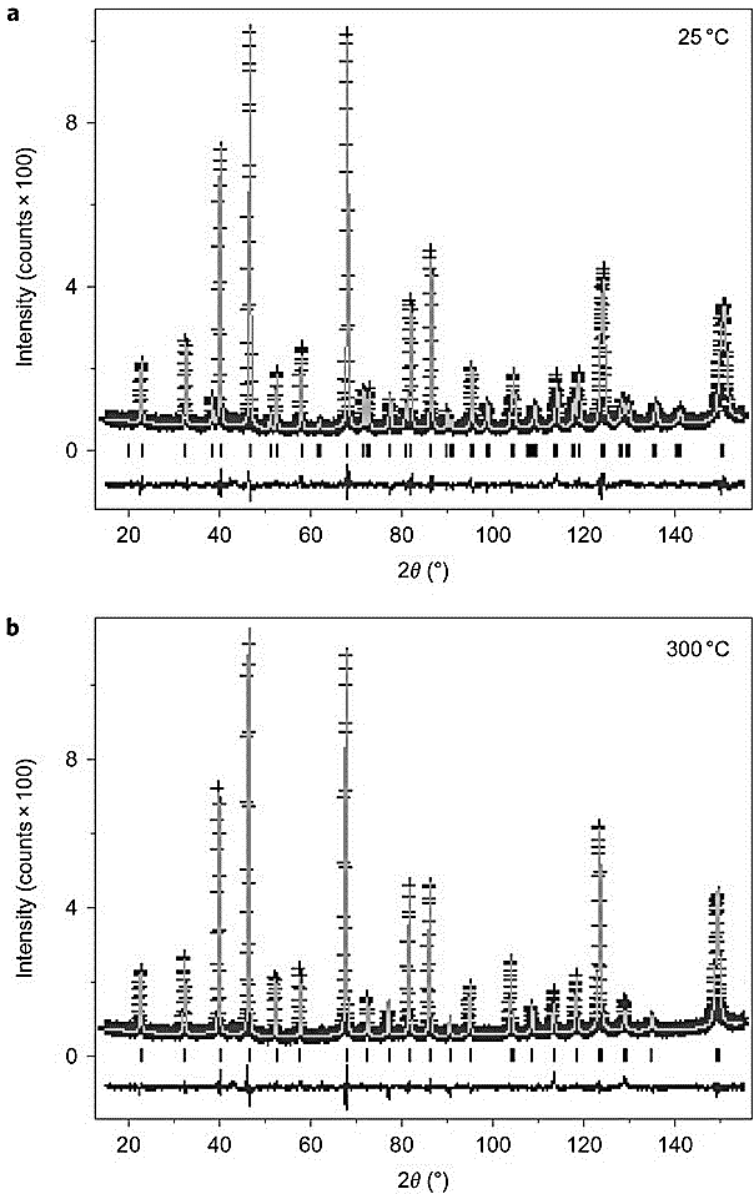

Figure 1. **Powder neutron diffraction patterns for $SrNbO_2N$.** Fits are shown with the observed points as crosses, calculated profiles as full lines and the difference and reflection markers offset below. The 300 °C fit

is of the pseudocubic (tetragonal *P*4/*mmm*) model inTable 1, with barely resolvable broadenings that arise from the anion order. Superstructure peaks caused by the rotational order of octahedra are evident at 25 °C, and the fit is of the constrained monoclinic *I*112/*m*model in Table 2.

Neutron diffraction is sensitive to small anion displacements because the scattering lengths of the light and heavy atoms are comparable, and it also offers high O/N scattering contrast (the neutron-scattering lengths *b* are b_{Sr} = 0.702 fm, b_{Nb} = 0.705 fm, b_{Ta} = 0.691 fm, b_O = 0.581 fm andb_N = 0.936 fm). However, the sensitivity of powder neutron data to anion order in a perovskite depends on the magnitude of the accompanying lattice distortion that broadens or splits the diffraction peaks. If the cell distortion is small, then O/N ordered and disordered models give very similar diffraction intensities, as confirmed by the simulated patterns shown in the Supplementary Information. Hence, although the high-temperature $SrMO_2N$ neutron data are fitted satisfactorily by a statistically disordered cubic perovskite model in which all the anion sites are equivalent, we also tested a tetragonal *P*4/*mmm* symmetry model to investigate possible long-range anion order.

Refinements of the *P*4/*mmm* model, which allows for possible 1:2 anion order over inequivalent sites X1 and X2, gave a striking result. For both $SrNbO_2N$ and $SrTaO_2N$, the fits converged to an ordered model with the X1 site fully occupied by O, and the X2 sites occupied by a near 50/50 O/N mixture, as shown in Table 1. For $SrNbO_2N$ the refined anion composition of $SrNbO_{2.07}N_{0.93}$revealed a small oxygen excess, consistent with the chemical analysis and previous studies of this phase[2, 10], and this composition was used in the fits to other diffraction profiles. $SrTaO_2N$ was found to be stoichiometric by analysis and neutron refinement. The slight decrease of the tetragonal *c*-dimension relative to the *a*-dimension is consistent with the anion order, as oxide is slightly smaller than nitride, but the lattice distortion is too small to result in visible peak broadenings and the anion segregation in the refinement is driven by the slight difference in intensities of the composite powder diffraction peaks, as illustrated by an improvement in the structure factor-squared residual (R_F^2) from 5.22 to 4.96% for the odd $h + k + l$ reflections, which are sensitive to the anion distribution. The oxygen occupancies of the X1 site decreased slightly with increasing temperature (Fig. 2b), but remained at ~90% up to the highest measured temperature of 750 °C for $SrTaO_2N$, which approached the synthesis conditions (≥900 °C) for this material[4]; this shows that the anion order is highly robust. Hence, we conclude that the high-temperature pseudocubic $SrMO_2N$ structures are tetragonal because of the well-defined $1O/2(O_{0.5}N_{0.5})$ anion order over the X1 and X2 sites, although the magnitude of the resultant tetragonal distortion is very small (c/a = 0.9993).

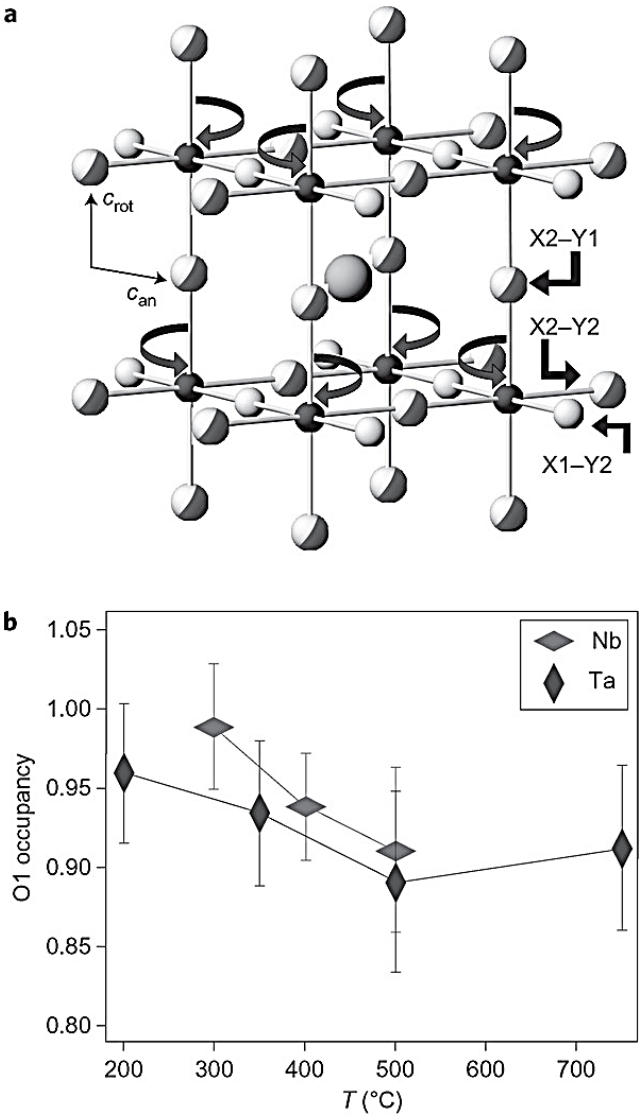

Figure 2. **Anion order in the $SrMO_2N$ perovskites. (a)** Structural model that shows the relationship between the unique axes for anion order (c_{an}) and octahedral rotation (c_{rot}) in the room-temperature phase. Shown is the correspondence between the X1 (oxide, unshaded atoms) and X2 (50/50 O/N, half-shaded) sites produced by anion order, and the inequivalent Y1 and Y2 sites created by rotational order. **(b)** The oxygen occupancies of the X1 site in the pseudocubic M = Nb and Ta phases at high temperatures.

Atom	***x***	***y***	***z***	U_{iso} (Å^2)	**O/N occupancy**
Sr	0.5	0.5	0.5	0.0170(5) *0.0130(5)*	
Nb *Ta*	0	0	0	0.0082(4) *0.0052(4)*	
X1	0	0	0.5	0.0225(4) *0.0187(3)*	0.99(4)/0.01 *0.96(4)/0.04*
X2	0.5	0	0	0.0225 *0.0187*	0.54(3)/0.46 *0.51(3)/0.49*

Results for $SrNbO_2N$ at 300 °C and for $SrTaO_2N$ (given in italics where different) at 200 °C; those for other temperatures are given in theSupplementary Information. Atomic coordinates (*x*, *y* and *z*) in tetragonal space group *P*4/*mmm*, isotropic thermal factors (U_{iso}) and refined O/N occupancies at the two anion sites are listed.

Estimated standard deviations in the independently refined parameters are in parentheses. Lattice parameters and agreement factors, $SrNbO_2N$: a = 4.0541(2) Å, c = 4.0511(4) Å, χ^2 = 4.12, R_{wp} = 5.61% (wp = weighted profile), R_F^2 = 3.30%; $SrTaO_2N$: a = 4.0442(3) Å, c = 4.0421(5) Å, χ^2 = 2.81, R_{wp} = 5.25%, R_F^2 = 3.62%.

Table 1. **Refined structures for the pseudocubic phases of $SrMO_2N$.**

On cooling to room temperature, $SrNbO_2N$ and $SrTaO_2N$ adopted a rotationally ordered perovskite superstructure (Fig. 2a). Rotation of the octahedra around a unique c axis created two anion sites in a 1/2 ratio, with Y1 on the c-axis and Y2 in the a–b plane, and the M–Y2–M bridge bent (with an angle 168.5° from the $SrNbO_2N$ refinement given below). Conventionally, this superstructure is described by the tetragonal space group $I4/mcm$ (refs 2,8,9,10), but our electron diffraction images of individual $SrMO_2N$ crystallites (Fig. 3) and the $EuMO_2N$ analogues (see Supplementary Information) consistently showed the presence of very weak ($h0l$) and ($0kl$) (h or k = odd) reflections that should be absent in $I4/mcm$. This lowering of symmetry may result from the anion ordering observed in the high-temperature phase if it has an orientational relationship to the rotational order.

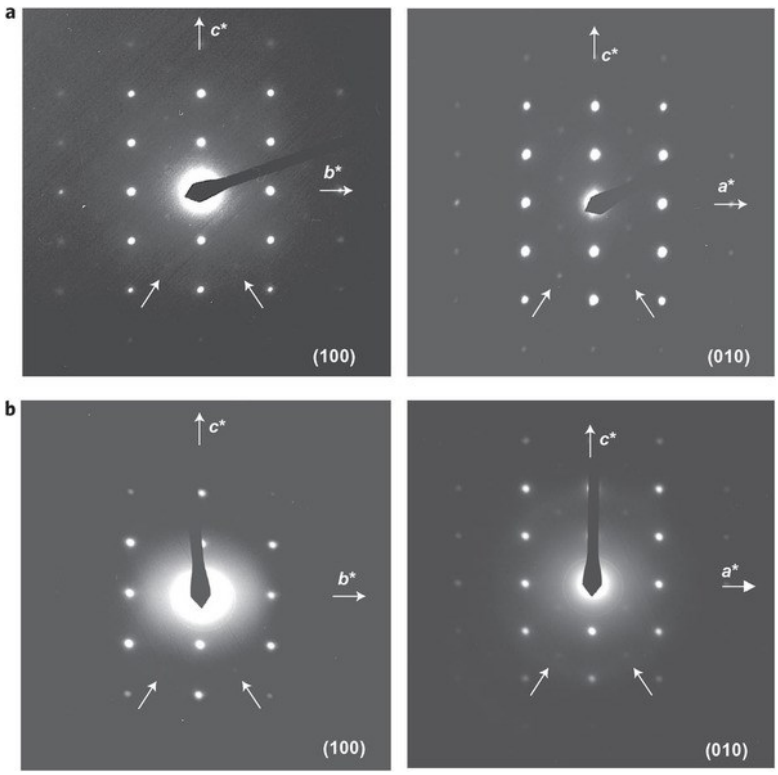

Figure 3. **Electron diffraction images of $SrMO_2N$ crystallites. (a), (b)** The (100) and (010) zones are shown for M = Nb (**a**) and M = Ta (**b**). The presence of weak ($0kl$) and ($h0l$) (k or h = odd) reflections (diagonal arrows) shows that the c-glide symmetry expected for the $I4/mcm$model of rotational order is broken by anion order.

Neutron refinement of the room-temperature O/N occupancies in the *I*4/*mcm* model gave a near 50/50 population at the Y1 site, which showed that this corresponds to one of the X2 sites in the high-temperature structure. This implies that the two Y2 sites in the room-temperature structure are not equivalent, as one should correspond to the X1 site (100% O) and the other should be the remaining X2 (50/50 O/N) site, as shown in Fig. 2a. This inequivalence lowers the space-group symmetry from tetragonal *I*4/*mcm* to monoclinic *I*112/*m* (a non-standard setting of *C*2/*m*) and we attempted to fit an *I*112/*m* model to the room-temperature neutron data (Table 2). No stable monoclinic refinement was possible for $SrTaO_2N$, and the model shown is equivalent to an *I*4/*mcm*description with O/N ratios of 50/50 at the Y1 site and an average 75/25 at the two Y2 positions. The same distributions were reported in previous studies of $SrTaO_2N$ (ref. 9) and $CaTaO_2N$ (ref. 8), in which further octahedral tilting lowered the apparent symmetry to orthorhombic *Pbnm* and anion order is predicted to result in a monoclinic $P112_1/m$ structure by analogy with the *I*112/*m*distortion.

Atom	***x***	***y***	***z***	U_{iso} **(Å^2)**	**O/N occupancy**
Sr	0	0.5	0.25	0.0094(4) *0.0085(4)*	
Nb1 *Ta1*	0	0	0	0.0069(3) *0.0039(4)*	
Nb2 *Ta2*	0	0	0.5	0.0069 *0.0039*	
Y1(X2)	0	0	0.25	0.0145(3) *0.0138(3)*	0.66/0.32 *0.48(4)/0.52*
Y2(X1)	0.7249(2) *0.7319(3)*	0.7751 *0.7681*	0	0.0145 *0.0138*	0.84(6)/0.16 *0.76/0.24*
Y2(X2)	0.7751 *0.7681*	0.2751 *0.2681*	0	0.0145 *0.0138*	0.57(6)/0.43 *0.76/0.24*

Results for $SrNbO_2N$ and $SrTaO_2N$ (given in italics where different) $\sqrt{2} \times \sqrt{2} \times 2$ rotational superstructures at room temperature are in monoclinic space group *I*112/*m*, but the refined cell parameters and atom positions were constrained by tetragonal *I*4/*mcm* symmetry. The anion labels show how the *I*4/*mcm* anion sites (Y) are related to those in the high-temperature model (X sites; see Fig. 2a). For $SrNbO_2N$, occupancies at the three anion sites were refined independently, subject to the overall composition $SrNbO_{2.07}N_{0.93}$. This was not possible for the $SrTaO_2N$ refinement and the two Y2 site occupancies were constrained as equal and subject to the stoichiometry $SrTaO_{2.00}N_{1.00}$. This refinement is equivalent to an *I*4/*mcm* fit. Lattice parameters and agreement factors, $SrNbO_2N$: $a = b = 5.7077(2)$ Å, $c = 8.1026(3)$ Å, $\gamma = 90°$, $\chi^2 = 3.78$, $R_{wp} = 5.22\%$, $R_F^2 = 3.78\%$; $SrTaO_2N$:$a = b = 5.7063(2)$ Å, $c = 8.0817(4)$ Å, $\gamma = 90°$, $\chi^2 = 2.64$, $R_{wp} = 5.00\%$, $R_F^2 = 4.16\%$.

Table 2. **Refined models for the rotational superstructures of $SrMO_2N$.**

For $SrNbO_2N$, it was possible to refine the occupation factors of the three anion sites independently, subject to the fixed overall composition, with lattice parameters and atomic positions constrained by *I*4/*mcm* symmetry. The results given in Table 2 support the above expectation as the Y2(X1) site has a high (87%) O occupancy, but the Y2(X2) site has an occupancy of 51% O. This anion order leads to the loss of the *c*-glide plane symmetry observed in the electron diffraction patterns (Fig. 3).

From the above refinements, we conclude that a robust $1O/2(O_{0.5}N_{0.5})$ anion order is present over the three available sites for $SrMO_2N$ (M = Nb, Ta) perovskites, up to at least ~1,000 K for M = Ta. The anion order controls the ordering of octahedral rotations below ~500 K, but the unique axis for anion order does not correspond to the unique axis for octahedral rotation (Fig. 2a). Although the anion order is well-defined, it results in very small metric distortions of the apparent high-temperature $Pm\bar{3}m$ and room temperature *I*4/*mcm* structures. High-resolution powder neutron diffraction data enabled the high-temperature *P*4/*mmm* (pseudocubic $Pm\bar{3}m$) structures to be refined freely, but this was not possible for the expected room-temperature *I*112/*m* models, which have *I*4/*mcm* pseudosymmetry. Further improvements may be possible using higher resolution powder diffraction data, but the O/N disorder over the two X2 sites resulted in an intrinsic strain broadening of diffraction peaks, which might limit the achievable resolution.

(ii) Structural principles

The neutron diffraction results show that a robust, partial anion order is present in the $SrMO_2N$ (M = Nb, Ta) perovskites over a wide temperature range, with oxide anions ordered on one axis of the pseudocubic cell with a 50/50 O/N mixture present on the other two. This distribution is difficult to rationalize from electrostatic repulsions between O^{2-} and N^{3-}, but is consistent with a well-defined, short-range order driven by covalent effects as follows.

Two strongly-bonded ligands in octahedral complexes of high valence d^0 transition-metal ions invariably adopt a *cis*- (90°) configuration to maximize $M(d_\pi)$–$X(p_\pi)$ covalency, such as in $Mo(NR)^{2+}_2$ (R = alkyl or aryl group) or MoO^{2+}_2 complexes[11, 12]. Hence, covalency favours the formation of *cis*-MN_2O_4 octahedra over the *trans*-(180°) arrangement in $SrMO_2N$ perovskites, as the nitride is bonded more strongly to the M cations than is the oxide. This is supported by electronic structure calculations for $ATaO_2N$ perovskites, which showed that *cis*-ordered structures have lower energies[13, 14], and by a pair-distribution function analysis of the total neutron scattering from $BaTaO_2N$, which found *cis*-coordination to be more likely than *trans*[15].

The combination of the *cis*-coordination of each M cation by two nitrides and the linear coordination of each nitride by two M cations results in the formation of zigzag –M–N– chains within the $SrMO_2N$ perovskites, as represented in Fig. 4. In an ideal, fully ordered structure, such as in Fig. 4a, the chains have a regular arrangement that gives rise to an anion-ordered superstructure in the *a*–*b*plane. However, zigzag –M–N– chains, like those of organic polymers, are very susceptible to disorder as there are two choices for the 90° turn at each M atom. This produces disordered chains and rings within the planes (Fig. 4b) and results in the average anion distribution observed in the neutron experiments, with an exact average 50/50 O/N composition at the *a*–*b* plane X2 anion sites because of the two *cis*-nitrides at each M site. On heating (for example, $SrTaO_2N$ to 750 °C), the ~10% occupancy of the *c*-axis X1 site by the nitride corresponds to the propagation of chains or rings between adjacent planes, as shown in Fig. 4c, which could lead to complete randomization

of the chains in all three dimensions at higher temperatures (Fig. 4d). Hence, even a true cubic AMO_2N perovskite with an average 67/33 O/N distribution at each site is expected to have well-defined local order with *cis*-MN_2O_4 octahedra at each site. Cubic superstructures of three-dimensionally ordered –M–N– chains are also possible, although these may be difficult to realize.

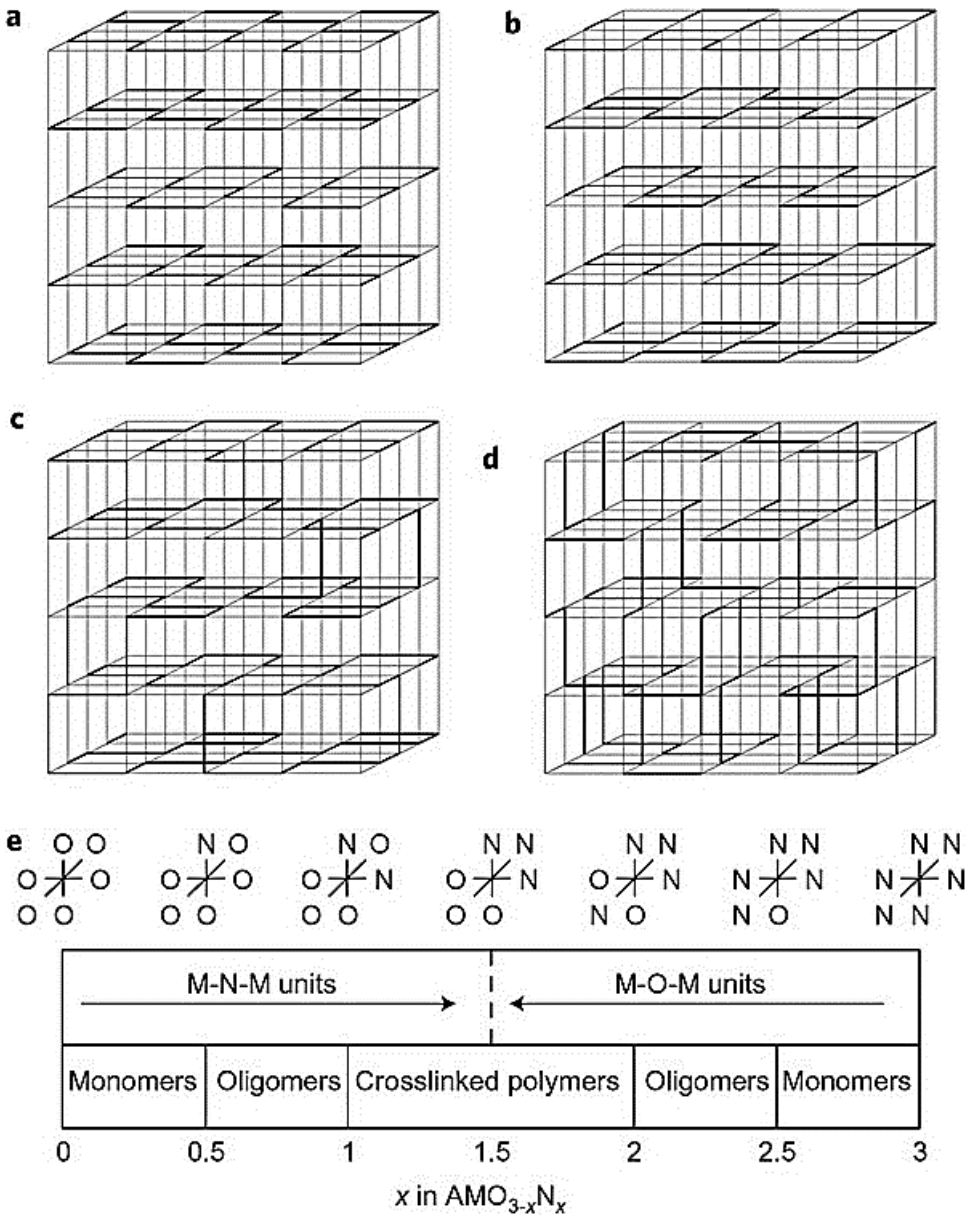

Figure 4. **Illustrations of *cis*-$(MX)_n$ (X = N,O) chain formations that arise from anion order in oxynitride perovskites. (a), (b)** An ideal two-dimensional order of chains **(a)**, but disorder leads to the statistical anion distribution observed in the pseudocubic phase of $SrNbO_2N$ at 300 °C **(b)**. **(c), (d)** At higher temperatures the partial occupation of the X1 site by the minority anion (for example, 10% nitride in $SrTaO_2N$ at 750 °C) corresponds to the chains jumping between successive planes **(c)**, and complete randomization results in average cubic symmetry with chains in all directions **(d)**. **(e)**, The local coordinations around M

cations and the degree of polymerization of M–X–M units for the range of $AMO_{3-x}N_x$ perovskites. In **(a–d)** heavy lines correspond to M–N–M units in AMO_2N types or to M–O–M units in $AMON_2$ types.

The two-dimensional (Fig. 4b) and three-dimensional (Fig. 4d) disordered –M–N– chains in AMO_2N perovskites provide well-constrained physical realizations of the self-avoiding walk (SAW) model in statistical mechanics[16]. The chain structures in AMO_2N correspond to a random journey on a square or cubic lattice with the constraints of visiting each point once and making a 90° turn at each point. SAW models were used extensively to describe the physical chemistry of linear polymers[17], and they should be applicable directly to the statistics of the –M–N– chains in AMO_2N perovskites. The anion orders can also be described by applying Pauling's ice rules for the local arrangements of protons in ice or magnetic moments in spin ices[18] to square or cubic lattices, in which M–N or M–O bonds, respectively, represent short or long O–H bonds or inward- or outward-pointing moments, but with the additional constraint that only *cis*-N–M–N connections are allowed. Pauling's famous estimate for the residual entropy (S) of ice is $S = R\ln(n/4)$, where $n = 6$ is the number of possible configurations per H_2O molecule and R is the molar gas constant. The same analysis on a square lattice with only *cis*-bonds has $n = 4$ so $S = 0$, which implies that a single long-range ordered state should form. Although this is intuitively incorrect, as the disordered configurations in Fig. 4b show, it demonstrates that the local chain structures are highly constrained despite the lack of long-range crystallographic order.

The above principle of local anion order driven by different M–N and M–O bond strengths predicts the local structure across the range of $AMO_{3-x}N_x$ perovskites. The preference for the more strongly bonded nitride ligands to be mutually *cis* results in a symmetry between nitride order in $AMO_{3-x}N_x$and oxide order in the corresponding AMO_xN_{3-x} composition. For example, greater M–N covalency favours the *cis*-MN_2O_4 arrangement in AMO_2N, described above, and also the *cis*-MN_4O_2octahedral configuration for $AMON_2$. This is verified by coordination complexes such as $MoO_2F_2(thf)_2$ (thf = tetrahydrofuran; ref. 19) and $Mo(N^tBu)_2Cl_2(py)_2$ (py = pyridine; ref. 20) in which the two most strongly-bonded anions (oxide or *t*-butylimido) are *cis*, as are the two most weakly bonded ligands thf or py. Hence, the representations of –M–N– chains in AMO_2N in Fig. 4 are equally applicable to –M–O– chains in $AMON_2$. This is corroborated by our observation of weak electron diffraction peaks that violate the *I*4/*mcm c*-glide symmetry for the rotationally ordered phase of $EuWON_2$ (see Supplementary Information), as for $SrMO_2N$ in Fig. 3. In addition, a recent low-temperature powder neutron diffraction study of $LaNbON_2$, which has orthorhombic *Pbnm*symmetry, gave O/N occupancies at the Y1- and Y2-type sites of 0.44(3)/0.56 and 0.28(2)/0.72, respectively (see the $SrMO_2N$ results in Table 2)[21], in excellent agreement with the predictions of our model. The observation that the disordered 50/50 O/N site occupies the Y1 position, which has the least displacive order, in the superstructures of both $SrMO_2N$ and $LaNbON_2$ shows that the coupling between anion and rotational or tilt orders is entropy-driven.

The $AMO_{3-x}N_x$ structures are described by the formation of M–N–M monomers within a perovskite oxide matrix as x increases from 0 to 0.5. These are connected into *cis*-oligomers and then infinite chains or rings at $x = 1$ and with *cis*-crosslinking for $1 < x < 1.5$ (Fig. 4e). This is mirrored by the creation of M–O–M monomers within a perovskite nitride matrix and their polymerization as $x$decreases from 3 to 1.5. At $x = 1.5$, facial (*fac*) MN_3O_3 octahedra in which the three nitrides or oxides are mutually *cis* are formed, by analogy with the *fac*-configuration observed in isolated $[MoO_3F_3]^{3-}$ complexes[22]. The *fac*-MN_3O_3 octahedra produce interpenetrating –M–N– and –M–O– networks of *cis*-crosslinked *cis*-chains in $AMO_{1.5}N_{1.5}$ perovskites.

Discussion

Although cation order–disorder phenomena in perovskites and other extended inorganic structures have been studied extensively, anion-order studies are much fewer, in particular for isoelectronic species such as oxide and nitride. Our results reveal a spontaneous, partial long-range order in $SrMO_2N$ (M = Nb, Ta) consistent with a robust, local anion order within MN_2O_4 octahedra. The key factor is the difference in M–N and M–O covalent bond strengths that results in a strong tendency for the *cis*-coordination of nitrides. The resulting –M–N– chains are intrinsically prone to disorder through the availability of several choices for the 90° turn at each M atom. Anion mobility in oxynitrides requires high temperatures, so careful annealing will be needed to attempt to prepare fully ordered structures such as those in Fig. 4a.

$SrNbO_2N$ and $SrTaO_2N$ are representative transition-metal oxynitride perovskites and so the same structural principles are expected to apply to other $AMO_{3-x}N_x$ phases, as shown in Fig. 4e, and to other extended oxynitride or oxyfluoride structures. For example, the perovskite-like layers of the K_2NiF_4-type oxynitrides Sr_2NbO_3N (ref. 23), Sr_2TaO_3N (ref. 24) and Ba_2TaO_3N (ref. 9) show 50/50 O/N anion occupancies that are likely to arise from disordered *cis*-chains, like those in the $SrNbO_2N$ and $SrTaO_2N$ analogues. A combination of average and local structural probes is needed to explore the wealth of expected structures, which are also amenable to modelling using statistical models such as SAW or Pauling ice rules. The M–O and M–N distances appear to be very similar because nitride has a slightly larger ionic radius than oxide, but this is compensated by a greater shortening associated with the more strongly covalent bonds to the transition metal. Hence, the metric distortions that arise from anion order are very small and highly resolved neutron diffraction data are needed to exploit the good O/N scattering contrast.

Anion order in oxynitrides is expected to have a strong influence on physical properties[26], especially when these are sensitive to local distortions. All the intermediate cation coordinations in $AMO_{3-x}N_x$ perovskites for $0 < x < 3$ (Fig. 4e) lack inversion symmetry, so off-centre M cation displacements and local dipoles result at each octahedron. Hence, the bulk materials are expected to have high dielectric constants, as reported for $BaTaO_2N$ (ref. 4). Simple ferroelectric orders, such as that in $BaTiO_3$, are less probable in the cubic oxynitride perovskites, as the spontaneous alternation of strong and weak bonds to equivalent anions in the former

material (schematically O · · · Ti–O · · · Ti–O) is likely to be suppressed by the formation of strong bonds to nitride and weak bonds to oxide in the latter (O · · · M–N–M · · · O), which tends to oppose local dipoles. However, the coupling of anion order to rotational or tilt order of octahedra, as we observed for $SrNbO_2N$ and $SrTaO_2N$, may result in structural arrangements that possess a net dipole. The absence of local inversion symmetry around the M cations (and A cations given the disorder of surrounding anion chains) may also increase significantly the intensities of optical transitions in pigments and luminescent oxynitride materials.

In conclusion, the structures of $SrNbO_2N$ and $SrTaO_2N$ evidence a well-defined local anion order with disordered *cis* –M–N– chains confined to planes within the three-dimensional perovskite framework. The anion order controls the axis around which the octahedra rotate to form a superstructure at room temperature. The anion order is robust, but the resultant lattice distortions are very small so that high-resolution neutron diffraction is needed to determine such structures. A wealth of similar local structures is expected across the range of $AMO_{3-x}N_x$ perovskites and further work is needed to establish their influence on structural and physical properties.

Methods

Polycrystalline samples (2 g) of $SrMO_2N$ (M = Nb, Ta) were prepared by reaction of stoichiometric amounts of $SrCO_3$ (99.9%, Baker) and Nb_2O_5 (99.99%, Aldrich) or Ta_2O_5 (99.99%, Aldrich) at 1,000 °C in NH_3(g) (99.9%, Carburos Metálicos) for several cycles of 40–50 hours, with pelletizing and intermediate regrinding. The flow rate of ammonia was 180 cm^3 min^{-1}. Syntheses of $EuNbO_2N$, $EuTaO_2N$ and $EuWON_2$ are described elsewhere[6, 7, 25]. Nitrogen contents were determined by combustion analysis using a Carlo Erba instrument. The resulting stoichiometries for the samples investigated by neutron and electron diffraction were $SrTaO_{1.99}N_{1.01}$, $SrNbO_{2.14}N_{0.86}$, $EuTaO_{1.94}N_{1.06}$, $EuNbO_{2.04}N_{0.96}$ and $EuWO_{0.96}N_{2.04}$.

Powder neutron diffraction data were collected using the Super-D2B diffractometer at the Institut Laue Langevin (ILL, Grenoble, France). Neutrons of wavelength 1.5943 Å were incident on an 8 mm vanadium can contained in a furnace. Patterns were collected at temperatures of 25–750 °C in the angular range $5 < 2\theta < 160°$ with steps of 0.05° and collection times of 3 hours.

Electron diffraction patterns from individual microcrystallites of the above oxynitride perovskites were obtained using a JEOL 1210 transmission electron microscope operating at 120 kV equipped with a side entry 60/30° double-tilt GATHAN 646 specimen holder. The samples were prepared by dispersing the powders in ethanol and depositing a droplet of this suspension on a carbon-coated holey film supported on a copper grid. To observe the diffraction intensities in the (100) and (010) planes, the sample stage was rotated about the *c*-axis of the pseudotetragonal (*I*4/*mcm*) superstructure.

References

[1] Asahi, R., Morikawa, T., Ohwaki, T., Aoki, K. & Taga, Y. Visible-light photocatalysis in nitrogen-doped titanium oxides. *Science* **293**, 269–271 (2001).

[2] Ebbinghaus S. G. *et al*. Perovskite-related oxynitrides – recent developments in synthesis, characterisation and investigations of physical properties. *Prog. Solid State Chem.* **37**,173–205 (2009).

[3] Jansen, M. & Letschert, H. P. Inorganic yellow–red pigments without toxic metals. *Nature* **404**,980–982 (2000).

[4] Kim, Y., Woodward, P. M., Baba-Kishi, K. Z. & Tai, C. W. Characterization of the structural, optical, and dielectric properties of oxynitride perovskites AMO_2N (A = Ba, Sr, Ca; M = Ta, Nb). *Chem. Mater.* **16**, 1267–1276 (2004).

[5] Highashi, M., Abe, R., Takata, T. & Domen, K. Photocatalytic overall water splitting under visible light using $ATaO_2N$ (A = Ca, Sr, Ba) and WO_3 in a IO_3^-/I^- shuttle redox mediated system. *Chem. Mater.* **21**, 1543–1549 (2009).

[6] Jorge, A. B. *et al*. Large coupled magnetoresponses in $EuNbO_2N$. *J. Am. Chem. Soc.* **130**,12572–12573 (2008).

[7] Yang, M., Oró-Solé, J., Kusmartseva, A., Fuertes, A. & Attfield, J. P. Electronic tuning of two metals and colossal magnetoresistances in $EuWO_{1+x}N_{2-x}$ perovskites. *J. Am. Chem. Soc.***132**, 4822–4829 (2010).

[8] Gunther, E., Hagenmayer, R. & Jansen, M. Strukturuntersuchungen an den oxidnitriden $SrTaO_2N$, $CaTaO_2N$ und $LaTaON_2$ mittels neutronen- und Röntgenbeugung. *Z. Anorg. Allg. Chem.* **626**, 1519–1525 (2000).

[9] Clarke, S. J., Hardstone, K. A., Michie, C. W. & Rosseinsky, M. J. High-temperature synthesis and structures of perovskite and n = 1 Ruddlesden–Popper tantalum oxynitrides. *Chem. Mater.* **14**, 2664–2669 (2002).

[10] Ebbinghaus, S. G., Weidenkaff, A., Rachel, A. & Reller, A. Powder neutron diffraction of $SrNbO_2N$ at room temperature and 1.5 K. *Acta Cryst. C* **60**, i91–i93 (2004).

[11] Tatsumi, K. & Hoffmann, R. Bent *cis* d^0 MO_2^{2+} vs. linear *trans* $d^0 f^0$ UO_2^{2+}: a significant role for nonvalence 6*p* orbitals in uranyl. *Inorg. Chem.* **19**, 2656–2658 (1980).

[12] Barrie, P., Coffey, T. A., Forster, G. D. & Hogarth, G. Bent vs linear imido ligation at the octahedral molybdenum(VI) dithiocarbamate stabilised centre. *J. Chem. Soc., Dalton Trans.*1999, 4519–4528.

[13] Fang, C. M. *et al*. Local structure and electronic properties of $BaTaO_2N$ with perovskite-type structure. *J. Phys. Chem. Solids* **64**, 281–286 (2003).

[14] Wolff, H. & Dronskowski, R. First-principles and molecular-dynamics study of structure and bonding in perovskite-type oxynitrides ABO_2N (A = Ca, Sr, Ba; B = Ta, Nb). *J. Comput. Chem.***29**, 2260–2267 (2008).

[15] Page, K. *et al*. Local atomic ordering in $BaTaO_2N$ studied by neutron pair distribution function analysis and density functional theory. *Chem. Mater.* **19**, 4037–4042 (2007).

[16] Madras, N. & Slade, G. *The Self-Avoiding Walk* (Birkhäuser, 1996).

[17] Van Rensburg, E. J. Statistical mechanics of directed models of polymers in the square lattice. *J. Phys. A* **36**, R11–R61 (2003).

[18] Bramwell, S. T. & Gingras, M. J. P. Spin ice state in frustrated magnetic pyrochlore materials.*Science* **294**, 1495–1501 (2001).

[19] Rhiel, M., Wocadlo, S., Massa, W. & Dehnicke, K. Reaktionen von MoNCl, und WNCl, mit elementarem fluor. Kristallstrukturen von $[MoO_2F_2(THF)_2]$ und $[WF_4(NCl)(CH_3CN)]$. *Z. Anorg. Allg. Chem.* **622**, 1195–1199 (1996).

[20] Chiu, H-T. *et al*. Syntheses and X-ray crystal-structures of dichlorobis(tert-butylimido) complexes of molybdenum(VI) – potential precursors to molybdenum nitride and molybdenum carbonitride. *J. Chin. Chem. Soc.* **41**, 755–761 (1994).

[21] Logvinovich, D. *et al*. Synthesis, crystal structure and optical properties of $LaNbON_2$. *Z. Anorg. Allg. Chem.* **636**, 905–912 (2010).

[22] Brink, F. J. *et al*. A combined diffraction (XRD, electron and neutron) and electrical study of $Na_3MoO_3F_3$. *J. Solid State Chem.* **174**, 450–458 (2003).

[23] Tobías, G. *et al*. Anion ordering and defect structure in Ruddlesden–Popper strontium niobium oxynitrides. *Inorg. Chem.*, **43**, 8010–8017 (2004).

[24] Diot, N. *et al*. Crystal structure determination of the oxynitride Sr_2TaO_3N. *J. Solid State Chem.***146**, 390–393 (1999).

[25] Kusmartseva, A. *et al*. Large magnetoresistances and non-ohmic conductivity in $EuWO_{1+x}N_{2-x}$. *Appl. Phys. Lett.* **95**, 022110 (2009).

[26] Fuertes, A. Synthesis and properties of functional oxynitrides – from photocatalysts to CMR materials. *Dalton Trans.* **39**, 5942–5948 (2010).